Tellus
SERIES B
CHEMICAL
AND PHYSICAL
METEOROLOGY
PUBLISHED BY THE INTERNATIONAL METEOROLOGICAL INSTITUTE IN STOCKHOLM

Tellus (2009), 61B, 747–755
Printed in Singapore. All rights reserved

TELLUS

On the observability of chemical and physical aerosol properties by optical observations: Inverse modelling with variational data assimilation

By MICHAEL KAHNERT*, *Swedish Meteorological and Hydrological Institute, 601 76 Norrköping, Sweden*

(Manuscript received 26 March 2009; in final form 2 July 2009)

ABSTRACT

Determining size-resolved chemical composition of aerosols is important for modelling the aerosols' direct and indirect climate impact, for source–receptor modelling, and for understanding adverse health effects of particulate pollutants. Obtaining this kind of information from optical remote sensing observations is an ill-posed inverse problem. It can be solved by variational data assimilation in conjunction with an aerosol transport model. One important question is how much information about the particles' physical and chemical properties is contained in the observations. We perform a numerical experiment to test the observability of size-dependent aerosol composition by remote sensing observations. An aerosol transport model is employed to produce a reference and a perturbed aerosol field. The perturbed field is taken as a proxy for a background estimate subject to uncertainties. The reference result represents the 'true' state of the system. Optical properties are computed from the reference results and are assimilated into the perturbed model. The assimilation results reveal that inverse modelling of optical observations significantly improves the background estimate. However, the optical observations alone do not contain sufficient information for producing a faithful retrieval of the size-resolved aerosol composition. The total mass mixing ratios, on the other hand, are retrieved with remarkable accuracy.

1. Introduction

Mapping and forecasting aerosol fields on regional and global scales is a problem with high relevance for air pollution monitoring as well as for climate research. Elevated concentrations of aerosols in ambient air have been demonstrated to result in increased morbidity and mortality (Dockery et al., 1993; Pope et al., 2009). The causes for the aerosols' adverse health effects are likely to be related to their size and/or chemical composition (Harrison and Yin, 2000).

To understand the complex interplay of meteorological, chemical and physical processes that determine the aerosols' formation, transport, transformation and deposition processes, one needs to analyse both size and chemical composition of the aerosol phase (Matta et al., 2003; Eleftheriadis et al., 2006). This will help to better understand the relation between ambient aerosol concentrations and emission sources, which is an important prerequisite for formulating effective abatement strategies.

Much attention has recently been paid to the role of aerosols in climate change (Lohmann and Lesins, 2002; Penner et al., 2004; Forster et al., 2007; Stier et al., 2007). The aerosol radiative properties, thus their direct impact on the radiative budget, are highly sensitive to size and chemical composition (Sokolik and Toon, 1999; Jacobson, 2001; Myhre and Stordal, 2001) and to particle morphology (Schulz et al., 1999, 1998; Kahnert, 2004; Kahnert and Kylling, 2004; Kahnert et al., 2005, 2007; Kahnert and Nousiainen, 2006; Nousiainen et al., 2006; Veihelmann et al., 2006). The first indirect aerosol forcing effect, that is, the aerosols' impact on cloud albedo, is determined by their hygroscopic properties. It has been argued that the aerosols' ability to act as cloud condensation nuclei is mainly depending on particle size (Dusek et al., 2006; Rosenfeld, 2006). A closer look reveals that this is largely true for aerosols larger than 200 nm with moderate amounts of soluble material, whereas droplet activation by aerosols in the size range between 40 and 200 nm strongly depends on their chemical composition and mixing state (McFiggans et al., 2006). Thus, obtaining reliable information on size-resolved aerosol composition is an essential step in constraining current estimates of the aerosol climate forcing effect, in understanding physical and chemical aerosol formation and transformation processes, and in studying the causes for adverse health effects related to particulate matter in ambient air.

Remote sensing observations of aerosols offer a reasonable spatial and temporal coverage combined with cost-effectiveness.

*Correspondence.
e-mail: michael.kahnert@smhi.se
DOI: 10.1111/j.1600-0889.2009.00436.x

However, extracting information about size-resolved chemical composition of aerosols from observations of optical and radiative properties is an ill-posed inverse problem. One way to solve inverse problems is by use of data assimilation techniques. Roughly speaking, the main idea of most data assimilation methods is to 'merge' information from the observations and from a background estimate of the state of the system. This is achieved by making use of additional information about the error variances and covariances of the state variables and of the observations such as to ensure that the 'merged' (analysed) state represents a maximum likelihood estimate of the state of the system. This method always provides an answer to the inverse problem. However, if observations are, for example, sparse in space or time, or if the observations contain too little information to constrain the state variables of the system, then the missing information is automatically supplemented by the background estimate. Thus, an important question is how much information is actually contained in the observations with regard to the configuration space in which we describe the state of the system.

In atmospheric chemistry applications, the background estimate can be obtained either from a climatological field of chemical tracers in the atmosphere, or, preferably, from a forecast computed with a chemical transport model. Chemical data assimilation of trace gases is a field of research that has been rapidly maturing over the previous years (Elbern et al., 1997; Elbern and Schmidt, 1999; Elbern et al., 2000; Elbern and Schmidt, 2001; Elbern et al., 2007; Constantinescu et al., 2007a,b). Application of chemical data assimilation to aerosol components is still evolving (Collins et al., 2001; Benedetti and Fisher, 2007; Kahnert, 2008). In the present paper we shall employ aerosol chemical data assimilation as an inverse modelling technique. The main question of this study is to what extent we can observe size-resolved chemical composition of aerosols by use of optical observations, such as aerosol optical depth (AOD), or vertical profiles of backscattering and extinction coefficients. The idea is to perform a controlled numerical experiment. The details of this approach are explained in Section 2. The numerical methods and tools are described in Section 3. Results are presented and discussed, respectively, in Sections 4 and 5.

2. Approach

Inverting remote sensing observations of aerosols by use of chemical data assimilation requires us to couple an aerosol chemical transport model (CTM) to an optical model. However, such a coupled system combines the sources of uncertainties of both constituents. Potential sources of error in a CTM are the emission fields, meteorological data, land-use data, boundary fields and initial fields, as well as simplifications in the description of the physical and chemical processes in the model itself. The optical model, on the other hand, needs to rely on simplifying assumptions about the particles' shape and mixing state, and, depending on the CTM, about the form of their size distribution. Thus, investigating the information contents of the observations in an operational retrieval system is complicated by the large number of potential error sources.

To circumvent such difficulties, the present study will focus on a controlled numerical experiment. The purpose is to investigate the observability of physical and chemical aerosol properties by remote sensing observations. A numerical experiment allows us to assume that the observations and the observation operator are virtually perfect. Under such conditions, a data assimilation algorithm will be able to reconstruct the true state of the system if the observations characterize the state of the system completely. However, if the information contained in the observations is incomplete, then the analysis result will, in general, deviate from the true state of the system. Thus, the strategy of our experiment is as follows:

(i) Perform a reference run of the aerosol transport model for a given set of input parameters to simulate the 'true' aerosol field. Further, compute aerosol optical properties from the resulting aerosol field to simulate 'observations' that are close to the true state of the system mapped into observation space.

(ii) Repeat the calculations with a perturbed set of input parameters to simulate a background estimate of the field that is impaired by uncertainties.

(iii) Perform a variational data analysis of the background aerosol fields by assimilating aerosol optical 'observations' obtained from the reference run.

(iv) Compare the analysis results with the reference results to assess to what extent the 'true' state can be reconstructed by inverse modelling of the 'observations' in conjunction with the background estimate. If the analysis result differs from the reference field, this will indicate that the information contained in the observations is incomplete.

For the reference run (i), we employ analysed meteorological input data. For the perturbed run (ii), we use 48-h forecasts. In either case, meteorological data are based on the High Resolution Limited Area Model (HIRLAM) (Gustafsson et al., 2001). Further, we perturb the input emissions as follows. All NO_x, NH_3 and black carbon (BC) emissions in the perturbed run (ii) are scaled by a factor of 1.25 as compared to the reference run (i). All SO_x, organic carbon (OC) and dust emissions are scaled by a factor of 0.75. As an example, Fig. 1 shows sulphate mixing ratios of aerosols in the third size class in the lowest model layer, computed on 24 July 2006 at 12:00 UTC. The left panel presents the results from the reference run (i), and the right panel shows the corresponding background field obtained with the perturbed meteorological and emission input data (ii). The figure illustrates clear differences between the two computations.

For the assimilation experiment (iii), we choose a location in Northern Germany at a latitude of 53.5° and a longitude of 10.0°. As can be seen in Fig. 1, the perturbed model underestimates the sulphate mass in the third size class as compared to

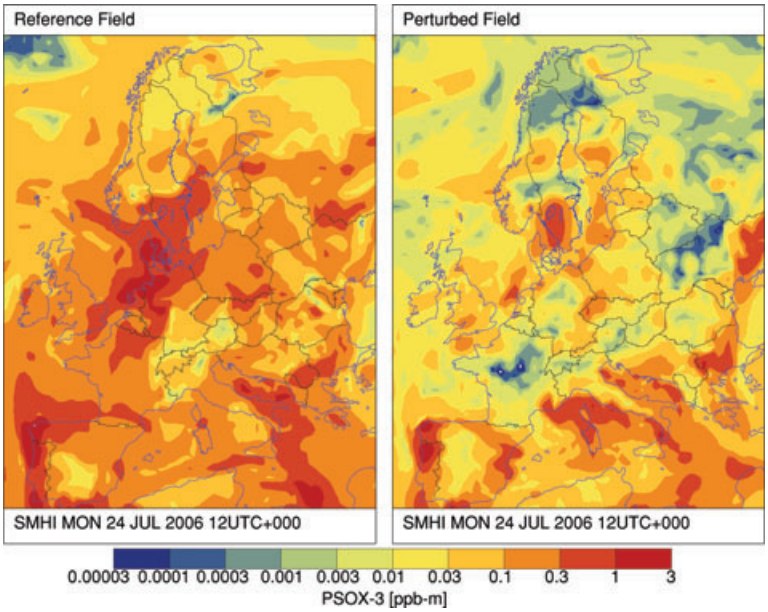

Fig. 1. Reference field (left) and perturbed field (right) for sulphate in the third size class (1.0–2.5 μm) in the lowest model layer.

the reference field by more than a factor of 10, which is a rather challenging case. Let us assume that we have observations of different aerosol optical properties at that location, which we simulate by computing these optical properties from the reference field. More specifically, we compute vertical profiles of the aerosol backscattering coefficient β_{sca} and the extinction coefficient k at the typical lidar wavelengths 355, 532 and 1064 nm. Also, we compute the AOD at typical sun-photometer wavelengths of 340, 380, 440, 500, 675, 870 and 1020 nm. Parts of or all of these observations are subsequently assimilated into the perturbed model. The 'observations' are assumed to be nearly perfect. This is achieved by assuming very low observational error variances. For β_{sca}, k and AOD the observational standard deviations are set to constant values of, respectively, 10^{-8}, 10^{-8} and $0.7 \cdot 10^{-4}$. This forces the analysis to produce results that follow the observational constraints faithfully.

Finally, in step (iv) the result of the assimilation, that is, the analysed aerosol field, is compared to the reference field. This comparison is performed in the configuration space of the model; that is, we compare the size-resolved chemical composition of the aerosols. The question we ask is if it is possible to retrieve the 'true' (reference) aerosol state by chemical data assimilation of optical observations. This is related to the question of how much information about the chemical and physical aerosol properties is contained in various amounts of optical observations. However, it is important to note that the ability to solve the inverse problem by data assimilation is not merely related to the intrinsic information contents of the assimilated observations. Rather, it is a property of the entire assimilation system. We shall return to this issue in Section 5.

It should also be emphasized that we formulate the retrieval question with respect to the configuration space of our CTM. Retrieving information about the size-resolved chemical composition of the aerosol phase is a highly ambitious goal. In other applications it may be perfectly sufficient to retrieve the lowest moments of the size distribution and the aerosols' refractive index (Mishchenko et al., 2007).

3. Methods

The CTM on which this study is based is the multiple-scale atmospheric transport and chemistry modelling system (MATCH) (Robertson et al., 1999; Foltescu et al., 2005; Andersson et al., 2007). It contains a photochemistry model with 64 prognostic components, a sea salt model and a dispersion model for primary emitted particles. The model computes mass mixing ratios of sulphate, nitrate, ammonium, sea salt, OC, BC and dust particles in four different size classes. The size classes cover particle diameters in the ranges [0.02, 0.1) μm, [0.1, 1.0) μm, [1.0, 2.5) μm and [2.5, 10.0) μm. The model is run with a horizontal resolution of 0.4°.

Aerosol optical properties are computed by use of the spherical particle and external mixture approximations. Refractive indices at different wavelengths for the different chemical constituents are taken from the OPAC database (Hess et al., 1998), where the OPAC refractive index for soluble particles has been used for ammonium, nitrate and OC particles. The details of the observation operators for coupling the CTM results to the optical observation parameters are reported by Kahnert (2008). Note that the same optics model is used to generate the synthetic 'observations' from the reference model, and to formulate the observation operator in the assimilation algorithm. Thus, the assimilation algorithm compares the reference field with the background estimate each mapped into observation space by use

of the same aerosol optics model. Uncertainties related to the formulation of the optics model are thereby neglected; that is, the aerosol optics model is assumed to be perfect in this numerical experiment.

The data analysis is performed by a multivariate three-dimensional variational method (3DVAR). A horizontal resolution of 0.8° is used for computing analysis increments. The analysis program is based on a spectral formulation (Berre, 2000). A modified NMC method (Parrish and Derber, 1992) is employed for modelling the background error covariances. They are, in general, non-separable in the horizontal and vertical directions. The background error correlations, but not the error covariances, are assumed to be homogeneous and isotropic in the horizontal dimensions. A detailed description of the MATCH-3DVAR assimilation system and of the background error statistics is given by Kahnert (2008).

4. Results

As a first result, we consider the aerosol mass mixing ratios $PM_{2.5}$ and PM_{10}, that is, the mass mixing ratios of particles smaller than 2.5 and 10 μm, respectively. These are diagnostic variables that are obtained by summation of the mass mixing ratios of the different chemical aerosol components in the corresponding size classes. Figure 2 shows a comparison of vertical profiles computed for the reference case (solid line), the perturbed results (dashed line) and the analysis results (dash-dotted line). The 3DVAR analysis results shown in Fig. 2 are based on assimilating only the backscattering coefficient $\beta_{\rm sca}$ at a single wavelength of 355 nm. Panel (a) presents results for $PM_{2.5}$ at the 'observation' site. One can see clear discrepancies between the reference case and the perturbed case. However, the 3DVAR analysis yields mass mixing ratios that agree remarkably well with the reference case. The analysis only slightly underestimates the reference results.

Panel (b) shows corresponding results for PM_{10}, which is also slightly underestimated near the ground. The analysis turns out to overestimate the coarse fraction $PM_{coarse} = PM_{10}$ - $PM_{2.5}$ (not shown). However, the coarse mass PM_{coarse} only contributes about 10% to the PM_{10} mass in this case, whereas $PM_{2.5}$ contributes about 90%. For this reason, the underestimation of $PM_{2.5}$ outweighs the overestimation of PM_{coarse}. Thus, the net effect is an underestimation of $PM_{10} = PM_{2.5} + PM_{coarse}$.

The method employed in this numerical experiment also allows for estimating the regional representativeness of the 'observed' $\beta_{\rm sca}$ profile. As we move away from the 'observation' site, the agreement between the analysis and the reference fields deteriorates. This is illustrated in panels (c) and (d), which show comparisons analogous to the ones in panel (a) for locations 100 and 500 km east of the observation site, respectively. In panel (c), the analysis result is still closer to the reference than to the perturbed case. In panel (d), the analysis lies somewhat closer to the perturbed case. These results suggest that, with regard to $PM_{2.5}$ mass retrieval, the lidar 'observations' have a radius of influence of a few hundred kilometres. This is largely controlled by the horizontal background error covariances employed in the assimilation algorithm, which are discussed in detail by Kahnert (2008).

Figure 3 presents mass mixing ratios of secondary inorganic aerosols (SIA) in the third size class. The SIA mass is obtained by summation of the sulphate, nitrate and ammonium mass mixing ratios. The reference and perturbed cases are represented by

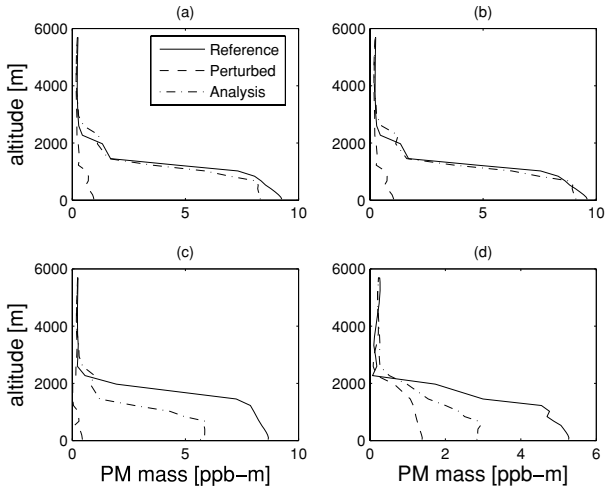

Fig. 2. (a) $PM_{2.5}$ as a function of altitude at the observation site (53.5°N, 10.0°E). The figure shows the reference case (solid line), the perturbed case (dashed line), and the 3DVAR analysis (dash-dotted line) based on assimilating $\beta_{\rm sca}$ at 355 nm. (b) As (a), but for PM_{10}. (c) As (a), but 100 km east of the observation site. (d) As (a), but 500 km east of the observation site.

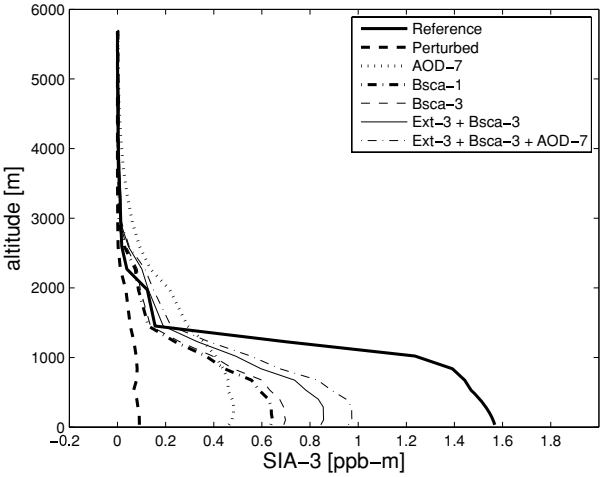

Fig. 3. Vertical profile of SIA mass mixing ratios in the third size class (1.0–2.5 μm) at 53.5°N, 10.0°E. The reference case and the perturbed case are compared to different assimilation experiments as described in the text.

the thick solid line and the thick dashed line, respectively. The perturbed case underestimates the SIA mass near the surface by roughly a factor of 16. The other curves depict results obtained from different assimilation experiments.

First, AOD 'observations' at seven different wavelengths have been assimilated. The analysis result is represented by the dotted line (labelled 'AOD-7' in the figure legend). One observes that the analysis yields a strong increase of the column SIA mass as compared to the background estimate (i.e. the perturbed case). However, the vertical distribution of the SIA mass is not well reproduced by the analysis. At lower altitudes, the analysis underestimates the SIA mass by almost a factor of 4. Above 1500 m, the analysis overestimates the reference case by roughly a factor of 2. Apparently, the perturbed case overestimates the effectiveness of the turbulent vertical mixing of the aerosols. The analysis simply scales the entire background estimate of the SIA mass profile without correcting the vertical distribution, since AOD observations only contain information integrated over the entire atmospheric column.

The situation is considerably improved by assimilating the simulated lidar observations. The thick dash-dotted line in Fig. 3 ('Bsca-1') represents analysis results obtained by assimilating a vertical profile of β_{sca} at 355 nm. The analysis yields a better representation of the vertical distribution of the SIA mass than that obtained by the AOD assimilation, although the reference case is still considerably underestimated. Assimilation of β_{sca} at three lidar wavelengths 355, 532 and 1064 nm ('Bsca-3', thin dashed line) only results in a small improvement of the analysis. More improvement can be achieved by simultaneously assimilating profiles of β_{sca} and of the extinction coefficient at those three wavelengths ('Ext-3 + Bsca-3', thin solid line). Extinction and backscattering observations can be performed with lidar instruments that also measure Raman scattering.

Finally, we consider the case of co-located extinction, backscattering and AOD observations. Thus, we assimilate extinction and backscattering profiles at the three lidar wavelengths, and AOD at the seven sun-photometer wavelengths. The analysis result is represented by the thin dash-dotted line ('Ext-3 + Bsca-3 + AOD-7'). We can see that the additional information obtained from the AOD observations improves the results as compared to the analysis based on assimilating extinction and backscattering observations only. Near the ground, the analysed SIA mass is a factor of 10 higher than the background estimate. However, it is still almost 40% lower than the reference case. Thus, assimilation of optical observations does yield a significant improvement of the SIA background estimate. However, although the latter assimilation experiment involves a significant amount of optical observations, the inverse modelling solution does not yield a faithful retrieval of the 'true' SIA mass profile.

It is interesting to note that the analysis mapped into observation space is in very good agreement with the assimilated 'observations'. As an example, Fig. 4 shows the analysis-equivalent backscattering coefficient at a wavelength of 355 nm as a function of altitude (solid line), and the 'observations' (symbols) generated from the reference run. The analysis follows the observations faithfully. The backscattering and extinction coefficients at all considered wavelengths display similarly good agreements. The seven different analysis-equivalent AOD values deviate from the 'observations' by only 0.6–2.7%. The close agreement between observations and analysis is a result of the small observational standard deviations we assumed in our experiment, which forces the analysis to closely follow the observational constraints. The idea was to mimic nearly perfect observations, thus to disregard observational uncertainties, which can complicate the interpretation of results in operational applications.

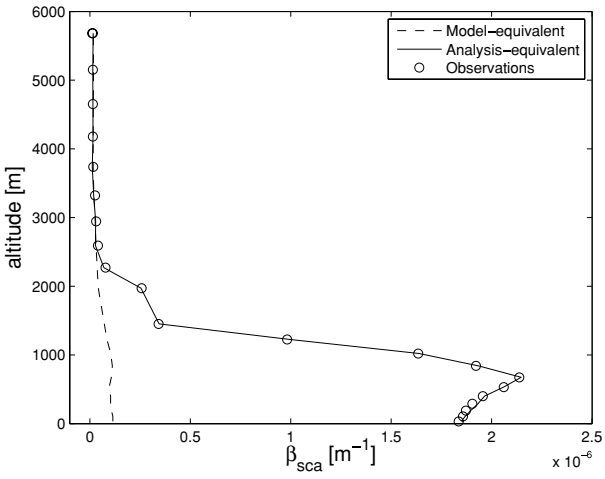

Fig. 4. Vertical profile of 'observed' backscattering coefficient at 355 nm (symbols), and corresponding model equivalent (dashed line) and analysis equivalent (solid line) at 53.5°N, 10.0°E.

Since co-located AOD and lidar observations are rare, we shall limit the discussion throughout the rest of the paper to the case labelled 'Ext-3 + Bsca-3', that is, the assimilation of vertical profiles of the extinction and backscattering coefficients at 355, 532 and 1064 nm. Figure 5 shows a comparison of the SIA mass profile for the reference case, background estimate and analysis for all four size classes. One observes that the analysis performs best in the lowest two size classes [panels (a) and (b)], in which it underestimates the reference case by about 25%. In the third size class [panel (c)], which had been studied in detail in Fig. 3, the analysis based on the assimilation experiment 'Ext-3 + Bsca-3' underestimates the reference case by roughly 50%. In the course mode, the analysis result lies almost 40% below the reference result.

Whereas the SIA mass is underestimated, the analysis turns out to overestimate the NaCl mass. Figure 6 shows a comparison of reference, background and analysis results for sodium chloride originating from sea salt. The analysis severely overestimates the NaCl mass mixing ratios for all four size classes. In fact, the difference between the reference case and the analysis

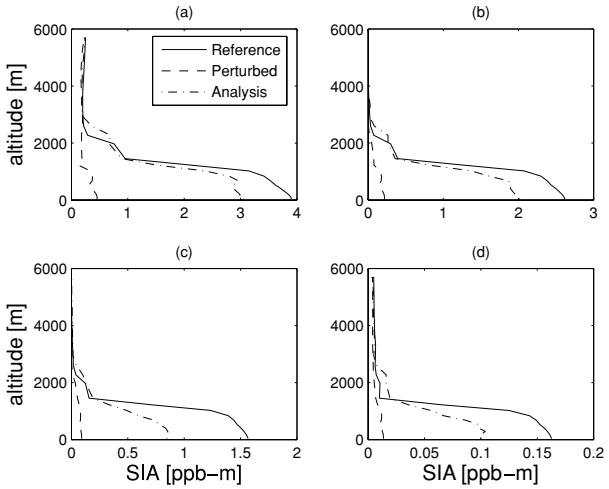

Fig. 5. Vertical profile of SIA mass mixing ratios in (a) size class 1 (0.02–0.1 μm), (b) size class 2 (0.1–1.0 μm), (c) size class 3 (1.0–2.5 μm) and (d) size class 4 (2.5–10.0 μm). The figure shows the reference case (solid line), the perturbed (background) case (dashed line) and the analysis result (dash-dotted line). The analysis is based on assimilating extinction and backscattering coefficients at three wavelengths. The observation site is located at 53.5°N, 10.0°E.

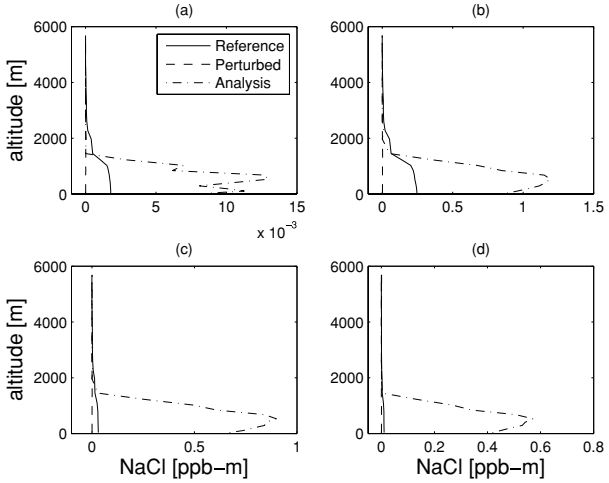

Fig. 6. As Fig. 5, but for NaCl.

is larger than the difference between the background and the reference results.

Figure 7 presents corresponding results for primary emitted particulate matter (PPM), namely BC (first row), OC (second row) and dust (third row) in the second size class (left column) and in the fourth size class (right column). The analysis agrees generally well with the reference case, even for those size classes not shown in the figure. The two notable exceptions are BC and dust in size class 4 [panels (b) and (f)]. The mixing ratio of coarse-mode BC is very low [note that the values on the x-axis are scaled by a factor of 10^{-5} in panel (b)]. Thus, the mismatch between the reference values and the analysis cannot be considered a serious issue in this case. The discrepancy between the analysed coarse-mode dust mixing ratio and the corresponding reference results in panel (f) is more severe.

The case studied here was characterized by background aerosol mixing ratios that deviated considerably from the reference case. We repeated the assimilation experiment for a different 'observation' location. We chose a site in Västergötland (southwestern Sweden) with a latitude of 58.0°N and a longitude of 13.0°E. According to Fig. 1, the ammonium sulphate mixing ratio in the third size class is comparable for the background (perturbed) field and the reference field in this area. As an example, Fig. 8 shows vertical SIA profiles analogous to those presented in Fig. 5 for the German site. Not surprisingly, it turns out that the absolute difference between the analysis and the reference result is smaller in this case, since the difference between the background field and the reference field is smaller in the first place. However, the analysis fails again to produce a faithful retrieval of the reference values of the mixing ratios. This confirms, as expected, that the quality of the background estimate is important for the quality of the analysis. However, it also underlines that the information contained in the optical observations is not sufficient for producing an unambiguous solution to the inverse problem.

5. Discussion and Outlook

The results presented in Section 4 revealed both strengths and limitations of inverse modelling of optical observations by chemical data assimilation. Generally speaking, there appears to be a great potential for improving model results by assimilating lidar and AOD observations. However, it appears unlikely that optical observations alone are sufficient to solve with high enough accuracy the inverse modelling problem in the configuration space of the CTM. Again, we emphasize that this conclusion is valid for the specific inverse modelling problem we are considering in this study.

Our results confirmed, not surprisingly, that a better background estimate yields a better solution to the inverse problem. Thus, it is clear that data assimilation is not a substitute for model development. Rather, assimilation and model development have to be considered as complementary to each other.

The ambiguity in the inverse problem originates from the fact that aerosol ensembles of different size-dependent chemical compositions can have similar optical properties. For instance, if we have a mixture of highly absorbing and weakly absorbing aerosols, and we reduce the former by a small amount and increase the latter by a sufficiently large amount, we may obtain a new aerosol mixture with similar absorption properties as the original ensemble. One usually tries to narrow down the possible solutions to the inverse problem by increasing the amount of information contained in the observations. This can be achieved, as we did in our study, by supplementing backscattering by extinction observations, or by increasing the number of wavelengths.

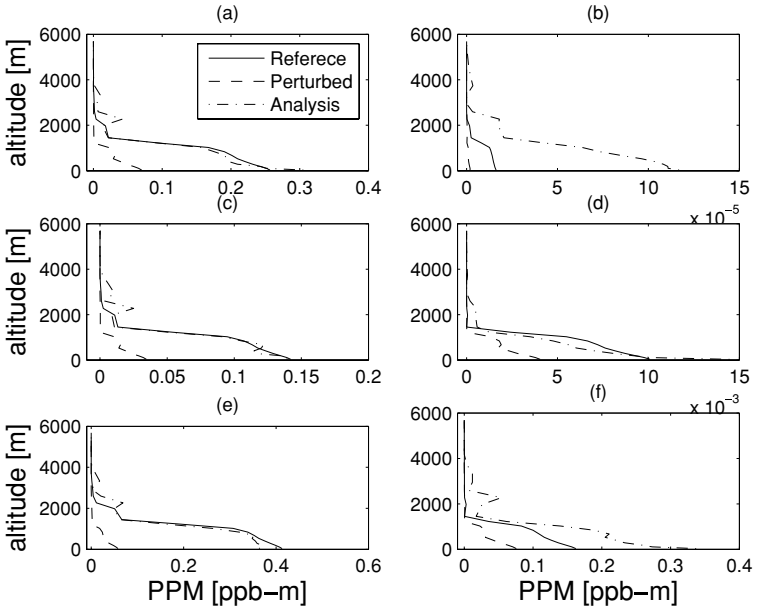

Fig. 7. As Fig. 5, but for BC (first row), OC (second row), and dust (third row), showing the second size class (0.1–1.0 μm, left column) and the fourth size class (2.5–10.0 μm, right column).

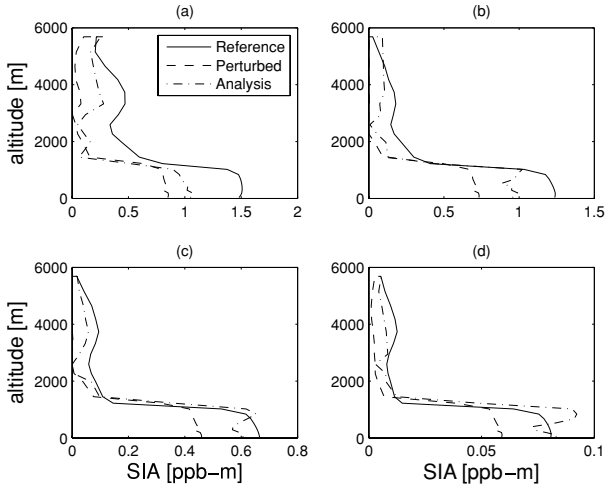

Fig. 8. As Fig. 5, but for a site in southwestern Sweden (58.0°N, 13.0°E).

The example of the SIA analysis shown in Fig. 3 clearly illustrated that this approach leads to a significant improvement of the inverse modelling solution, but not to a sufficiently accurate retrieval of the reference solution.

Gases in the atmosphere often have narrow absorption lines that can be exploited to design observations that target specific types of molecules. Aerosol components, on the other hand, usually lack such optical resonance features. The real and imaginary parts of the refractive indices of aerosol species are typically fairly smooth functions of the wavelength. Although there do exist differences between the optical properties of different chemical aerosol species, the results of our study suggest that these differences are not sufficiently distinct for removing the ambiguities in our specific inverse modelling problem.

As already indicated in Section 2, our ability to invert aerosol optical observations by chemical data assimilation is not just an intrinsic property of the observations themselves. A data assimilation system complements the information contained in the observations by a background estimate and by background error statistics. The analysis program first computes innovations, that is, differences between observations and background values mapped into observation space. Next, the analysis corrects the background field based on the innovations. How the information from the innovations is distributed back to the different model variables, and how it is horizontally and vertically spread out from the observation site into the surrounding space, is determined by the background error covariance matrix. Thus, the description of background error statistics is a critical factor in our ability to perform inverse modelling with chemical data assimilation. Another factor is the data assimilation method itself.

The 3DVAR method employed in this study assimilates observations sequentially. By contrast, the 4DVAR method assimilates observations over an entire time window, which is known to yield better results. However, the model adjoint required in the 4DVAR method is considerably more complex to implement and requires substantial computational resources. Adjoint aerosol dynamic models have recently been reported by Sandu et al. (2005).

Both the 3DVAR and the 4DVAR methods employ a constant background error covariance matrix. By contrast, methods based on the Kalman filter (Jazwinski, 2007), such as the Ensemble Kalman filter (Evensen, 2007), take the temporal evolution of the background error covariance matrix into account. Using the background error statistics ‘of the day’ in inverse modelling

may be an advantage if the error correlations between different chemical components or spatial error correlations are strongly time-dependent.

It seems highly plausible that more sophisticated data assimilation methods offer, for the price of more computational resources, much potential for further improvements. However, some of the results in Section 3, notably those obtained for SIA and NaCl, suggest that there exist certain problems that will be hard to tackle without assimilating additional information from other measurements. For instance, one should consider assimilating observations of aerosol precursor gases. This may help to constrain the SIA fraction.

Another important issue is the uncertainty of the emission input data. There is evidence suggesting that parameter estimation of emissions by data assimilation techniques can improve the forecasting ability of a CTM (Elbern et al., 2007). The approach described in this paper could be employed to systematically test the feasibility of inverse modelling of emissions by chemical data assimilation, and to identify observational parameters and network requirements for such a task. Constraining input emissions could greatly improve the accuracy of the background estimate, thus reduce difficulties in the inverse modelling of aerosol optical observations.

Finally, note that the optics model employed in this study is based on the external mixture approximation, which results in linear optical observation operators (Kahnert, 2008). A more realistic optics model would treat the different aerosol components as internally mixed. This would result in nonlinear observation operators, which may be more sensitive to changes in chemical composition, thus facilitating a discrimination among different aerosol mixtures based on different optical observations. However, nonlinearities also tend to complicate the treatment of the observation operator in the analysis algorithm.

6. Acknowledgments

This work was supported by the Swedish Research Council under contract number 80438701, and by the Swedish Governmental Agency for Innovation Systems (VINNOVA) as part of the AMAGAL project (2006-02314). Three anonymous reviewers are acknowledged for helpful suggestions.

References

Andersson, C., Langner, J. and Bergström, R. 2007. Interannual variation and trends in air pollution over Europe due to climate variability during 1958–2001 simulated with a regional CTM coupled to the ERA40 reanalysis. *Tellus* **59B**, 77–98.

Benedetti, A. and Fisher, M. 2007. Background error statistics for aerosols. *Q. J. R. Meteorol. Soc.* **133**, 391–405.

Berre, L. 2000. Estimation of synoptic and mesoscale forecast error covariances in a limited-area model. *Mon. Wea. Rev.* **128**, 644–667.

Collins, W. D., Rasch, P. J., Eaton, B. E., Khattatov, B. V. and Lamarque, J.-F. 2001. Simulating aerosols using a chemical transport model with assimilation of satellite aerosol retrievals: Methodology for INDOEX. *J. Geophys. Res.* **106**, 7313–7336.

Constantinescu, E. M., Sandu, A., Chai, T. and Carmichael, G. R. 2007a. Ensemble-based chemical data assimilation. I: General approach. *Q. J. Roy. Meteorol. Soc.* **133**, 1229–1243.

Constantinescu, E. M., Sandu, A., Chai, T. and Carmichael, G. R. 2007b. Ensemble-based chemical data assimilation. II: Covariance localization. *Q. J. Roy. Meteorol. Soc.* **133**, 1245–1256.

Dockery, D., Pope, C., XU, X., Spengler, J., Ware, J., et al, 1993. An association between air-pollution and mortality in 6 United-States cities. *N. Engl. J. Med.* **329**(24), 1753–1759.

Dusek, U., Frank, G. P., Hildebrandt, L., Curtius, J., Schneider, J., et al, 2006. Size matters more than chemistry for cloud-nucleation ability of aerosol particles. *Science* **312**, 1375–1378.

Elbern, H. and Schmidt, H. 1999. A four-dimensional variational chemistry data assimilation scheme for Eulerian chemistry transport modeling. *J. Geophys. Res.* **104**, 18 583–18 598.

Elbern, H. and Schmidt, H. 2001. Ozone episode analysis by four-dimensional variational chemistry data assimilation. *J. Geophys. Res.* **106**, 3569–3590.

Elbern, H., Schmidt, H. and Ebel, A. 1997. Variational data assimilation for tropospheric chemistry modeling. *J. Geophys. Res.* **102**, 15 967–15 985.

Elbern, H., Schmidt, H., Talagrand, O. and Ebel, A. 2000. 4D-variational data assimilation with and adjoint air quality model for emission analysis. *Environ. Model. Software* **15**, 539–548.

Elbern, H., Strunk, A., Schmidt, H. and Talagrand, O. 2007. Emission rate and chemical state estimation by 4-dimensional variational inversion. *Atmos. Chem. Phys.* **7**, 3749–3769.

Eleftheriadis, K., Colbeck, I., Housiadas, C., Lazaridis, M., Mihalopoulos, N., et al, 2006. Size distribution, composition and origin of the submicron aerosol in the marine boundary layer during the eastern mediterranean SUB-AERO experiment. *Atmos. Env.* **40**, 6245–6260.

Evensen, G. 2007. *Data Assimilation – the Ensemble Kalman Filter.* Springer, Berlin.

Foltescu, V., Pryor, S. C. and Bennet, C. 2005. Sea salt generation, dispersion and removal on the regional scale. *Atmos. Environ.* **39**, 2123–2133.

Forster, P., Ramaswamy, V., Artaxo, P., R. Betts, T. B., Fahey, D., et al, 2007. Changes in atmospheric constituents and in radiative forcing. In: *Climate Change 2007: The Physical Science Basis*, (eds. S. Solomon, D. Qin, M. Manning, Z. Chen, M. Marquis, K. Averyt, M. Tignor and H. Miller), Contribution of Working Group I to the Fourth Assessment Report of the Intergovernmetal Panel on Climate Change, Cambridge University Press, Cambridge.

Gustafsson, N., Berre, L., Hörnquist, S., Huang, X.-Y., Lindskog, M., et al, 2001. Three-dimensional variational data assimilation for a limited area model part I: General formulation and the background error constraint. *Tellus* **53A**, 425–446.

Harrison, R. and Yin, J. 2000. Particulate matter in the atmosphere: which particle properties are important for its effects on health? *Sci. Total Environ.* **249**(1–3), 85–101.

Hess, M., Koepke, P. and Schult, I. 1998. Optical properties of aerosols and clouds: The software package OPAC. *Bull. Am. Met. Soc.* **79**, 831–844.

Jacobson, M. Z. 2001. Global direct radiative forcing due to multicomponent anthropogenic and natural aerosols. *J. Geophys. Res.* **106**, 1551–1568.

Jazwinski, A. H. 2007. *Stochastic Processes and Filtering Theory*. Dover, Mineola.

Kahnert, F. M. 2004. Reproducing the optical properties of fine desert dust aerosols using ensembles of simple model particles. *J. Quant. Spectrosc. Radiat. Transfer* **85**, 231–249.

Kahnert, M. 2008. Variational data analysis of aerosol species in a regional CTM: Background error covariance constraint and aerosol optical observation operators. *Tellus* **60B**, 753–770.

Kahnert, M. and Kylling, A. 2004. Radiance and flux simulations for mineral dust aerosols: Assessing the error due to using spherical or spheroidal model particles. *J. Geophys. Res.* **109**, D09203, doi:10.1029/2003JD004318, errata: doi:10.1029/2004JD005311.

Kahnert, M. and Nousiainen, T. 2006. Uncertainties in measured and modelled asymmetry parameters of mineral dust aerosols. *J. Quant. Spectrosc. Radiat. Transfer* **100**, 173–178.

Kahnert, M., Nousiainen, T. and Veihelmann, B. 2005. Spherical and spheroidal model particles as an error source in aerosol climate forcing and radiance computations: A case study for feldspar aerosols. *J. Geophys. Res.* **110.** doi: 10.1029/2004JD005558.

Kahnert, M., Nousiainen, T. and Räisänen, P. 2007. Mie simulations as an error source in mineral aerosol radiative forcing calculations. *Q. J. R. Met. Soc.* **133**, 299–307.

Lohmann, U. and Lesins, G. 2002. Stronger constraints on the anthropogenic indirect aerosol effect. *Science* **298**, 1012–1014.

Matta, E., Facchini, M., Decesari, S., Mircea, M., Cavalli, F., et al, 2003. Mass closure on the chemical species in size-segregated atmospheric aerosol collected in an urban area of the Po Valley, Italy. *Atmos. Chem. Phys.* **3**, 623–637.

McFiggans, G., Artaxo, P., Baltensperger, U., Coe, H., Facchini, M. C., et al, 2006. The effect of physical and chemical aerosol properties on warm cloud droplet activation. *Atmos. Chem. Phys.* **6**, 2593–2649.

Mishchenko, M. I., Cairns, B., Kopp, G., Schueler, C., Fafaul, B. A., et al, 2007. Accurate monitoring of terrestrial aerosols and total solar irradiance: Introducing the Glory mission. *Bull. Am. Met. Soc.* **88**, 677–691.

Myhre, G. and Stordal, F. 2001. Global sensitivity experiments of the radiative forcing due to mineral aerosols. *J. Geophys. Res.* **106**, 18193–18204.

Nousiainen, T., Kahnert, M. and Veihelmann, B. 2006. Light scattering modeling of small feldspar aerosol particles using polyhedral prisms and spheroids. *J. Quant. Spectrosc. Radiat. Transfer* **101**, 471–487.

Parrish, D. F. and Derber, J. C. 1992. The National Meteorological Centre's spectral statistical interpolation analysis system. *Mon. Wea. Rev.* **120**, 1747–1763.

Penner, J. E., Dong, X. and Chen, Y. 2004. Observational evidence of a change in radiative forcing due to the indirect aerosol effect. *Nature* **427**, 231–234.

Pope, C. A., Ezzati, M. and Dockery, D. W. 2009. Fine-particulate air pollution and life expectancy in the United States. *N. Engl. J. Med.* **360**(4), 376–386.

Robertson, L., Langner, J. and Enghardt, M. 1999. An Eulerian limited-area atmospheric transport model. *J. Appl. Meteorol.* **38**, 190–210.

Rosenfeld, D. 2006. Aerosols, clouds, and climate. *Science* **312**, 1323–1324.

Sandu, A., Liao, W., Henze, D. K., Carmichael G. R. and Seinfeld, J. H. 2005. Inverse modeling of aerosol dynamics using adjoints: Theoretical and numerical considerations. *Aerosol Sci. Technol.* **39**), 677–694.

Schulz, F. M., Stamnes, K. and Stamnes, J. J. 1998. Modeling the radiative transfer properties of media containing particles of moderately and highly elongated shape. *Geophys. Res. Lett.* **25**, 4481–4484.

Schulz, F. M., Stamnes, K. and Stamnes, J. J. 1999. Shape-dependence of the optical properties in size-shape distributions of randomly oriented prolate spheroids, including highly elongated shapes. *J. Geophys. Res.* **104**, 9413–9421.

Sokolik, I. N. and Toon, O. B. 1999. Incorporation of mineralogical composition into models of the radiative properties of mineral aerosols from UV to IR wavelengths. *J. Geophys. Res.* **104**, 9423–9444.

Stier, P., Seinfeld, J. H., Kinne, S. and Boucher, O. 2007. Aerosol absorption and radiative forcing. *Atmos. Chem. Phys.* **7**, 5237–5261.

Veihelmann, B., Nousiainen, T., Kahnert, M. and van der Zande, W. 2006. Light scattering by small feldspar particles simulated using the Gaussian random sphere geometry. *J. Quant. Spectrosc. Radiat. Transfer* **100**(1–3), 393–405.